



LAWRENCE  
LIVERMORE  
NATIONAL  
LABORATORY

# Bounds on the Information Carrying Capacity of Pn Waves

D. B. Harris

December 4, 2008

## **Disclaimer**

---

This document was prepared as an account of work sponsored by an agency of the United States government. Neither the United States government nor Lawrence Livermore National Security, LLC, nor any of their employees makes any warranty, expressed or implied, or assumes any legal liability or responsibility for the accuracy, completeness, or usefulness of any information, apparatus, product, or process disclosed, or represents that its use would not infringe privately owned rights. Reference herein to any specific commercial product, process, or service by trade name, trademark, manufacturer, or otherwise does not necessarily constitute or imply its endorsement, recommendation, or favoring by the United States government or Lawrence Livermore National Security, LLC. The views and opinions of authors expressed herein do not necessarily state or reflect those of the United States government or Lawrence Livermore National Security, LLC, and shall not be used for advertising or product endorsement purposes.

This work performed under the auspices of the U.S. Department of Energy by Lawrence Livermore National Laboratory under Contract DE-AC52-07NA27344.

# Bounds on the Information Carrying Capacity of Pn Waves

D. B. Harris

## Abstract

Upper and lower bounds on the capacity of the Pn wave to transmit information about source identity are developed using models and measurements of Pn spatial signal structure across the ARCES array. The results show a very significant increase in information carrying capacity when contrasting observed propagation conditions with idealized free-space propagation. In essence, scattering greatly increases Pn channel capacity. As shown in a previous contribution, this increase in information can be captured with matched field calibrations and exploited to resolve sources more closely spaced than the Rayleigh resolution limit. These results mirror practices in cellular telephony that use arrays at the transmitter and receiver to exploit scattering for increased channel capacity.

## Introduction

Seismologists have an intuitive notion that the rich scattering environment of seismic wave propagation imprints unique spatial signatures on seismic wavefields that can be exploited for many applications involving repeating events. This contribution formalizes this notion by providing a graphic depiction of the scattering footprint on the ARCES array for the first-arriving P wave. Then measured spatial signal structure is contrasted with idealized spatial structure to estimate formally the increase in information carrying capacity afforded by scattering.

Calculations of information carrying capacity are scenario dependent. In the seismic scenario considered here a collection of closely-spaced mines in the Kola Peninsula of northwest Russia plays the role of transmitter and the ARCES seismic array in northern Norway, the role of receiver [Figure 1]. The information to be transmitted is which mine conducted an explosion. The signal received is the seismic waveform observed by ARCES for the explosion event in question. To formalize the estimation of channel capacity for this scenario, imagine the state of the mines is summarized by a random index variable which assumes a unique value indicating the mine at which a particular explosion was conducted [Figure 2]. In this contribution, a model for the joint probability of the value of the index variable and the corresponding observed seismic signal is developed. This probability model is used to estimate (actually bound) the mutual information between the transmitter and receiver, a measure of information carrying capacity which describes what knowledge of the observed signals tells us about the state of the mines.

Mutual information can be estimated for different assumed receiver signal models. In this contribution, simple plane-wave models for free-space Pn wave propagation are considered on the one hand, and measured covariance structure for the Pn wave are used on the other. The mutual information is estimated for both cases and compared. As we

will see, mutual information is significantly greater when the measured covariance structure is assumed, indicating a much greater information carrying capacity in the real-world case of a rich scattering environment.

In general, and in our particular application, it is not possible to evaluate the mutual information directly. However, it is possible to evaluate upper and lower bounds on the mutual information. These bounds are sufficiently tight to permit meaningful comparisons of information carrying capacity under different propagation conditions.

This contribution limits consideration of the seismic wavefield to the Pn phase, in fact, to a short data window that encompasses just the direct Pn wave, excluding Pn coda. This limitation simplifies the analysis, since the theoretical description of wave propagation need consider only a single mode describing free-space propagation. The estimated values of mutual information in this case suggest that event origins cannot be estimated reliably, except perhaps at very large signal-to-noise ratios (SNR). This observation is consistent with the fact that the mines are separated by less than the classical (Rayleigh) resolution limit for Pn when viewed from the ARCES array. However, when the measured Pn array signal covariance is used in the probability model the prediction is that explosion origins can be successfully distinguished. This result is remarkable, considering that only a small portion of the seismogram is used (inter-phase time differences are not considered), that a single array is employed, and that the mines are separated in some instances by only a few tenths of a degree in azimuth.

This contribution is organized in three sections. The first describes a frequency domain representation for the observed signals that we use to suppress the temporal structure of the signals which is variable from event to event and not diagnostic of the origin of the events. Information about the event origins is encoded in the spatial covariance structure of the signals observed in narrow frequency bands. The second section describes the estimation of spatial covariance for each of the ten mines in a range of frequency bands and shows that observed signal structure varies significantly among the mines, while theoretical structure is uniform. Finally, in the third section, the estimated and theoretical signal covariances are used to define a joint probability model between the index variable describing explosion origins at the mines and the observed signal. This probability model is used to estimate the information carrying capacity of Pn waves under both idealized and realistic conditions of propagation.

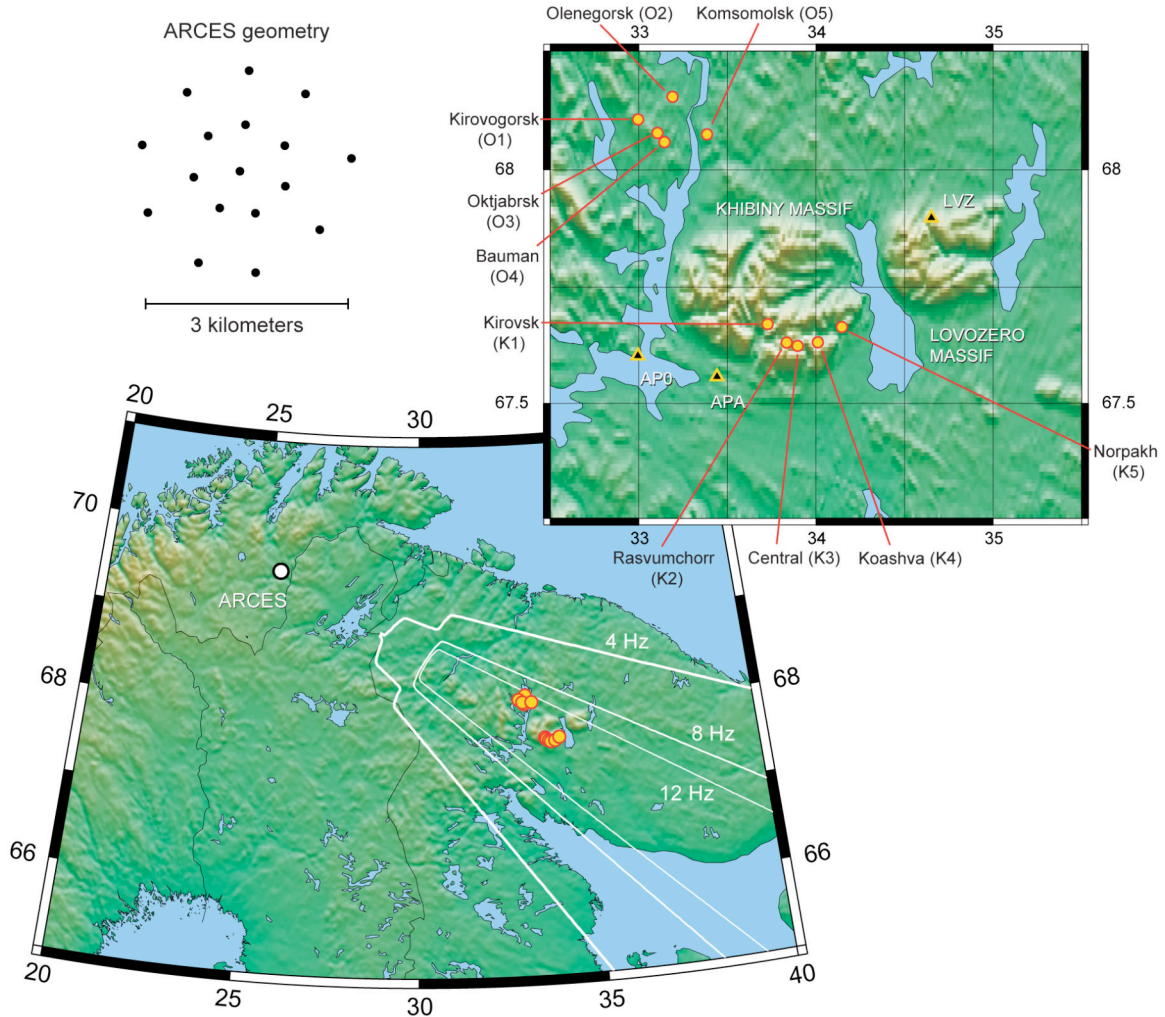


**Figure 1** The mines of the Khibiny and Olenegorsk regions provide an opportunity to calculate the information capacity of seismic propagation. The requirement met by these mines is that they constitute a very dense set of ground-truth sources. More widely spaced sources would not test the limits of array resolution and would yield trivial estimates of information capacity. The figure at bottom left shows the array pattern of the ARCES when steered to one particular mine (K2: Rasvumchorr) projected onto the geographic field of observation. The white lines are half-power contours and provide a common measure of resolution. Note that all of the mines fall within these contours, even at high frequencies (12 Hz).

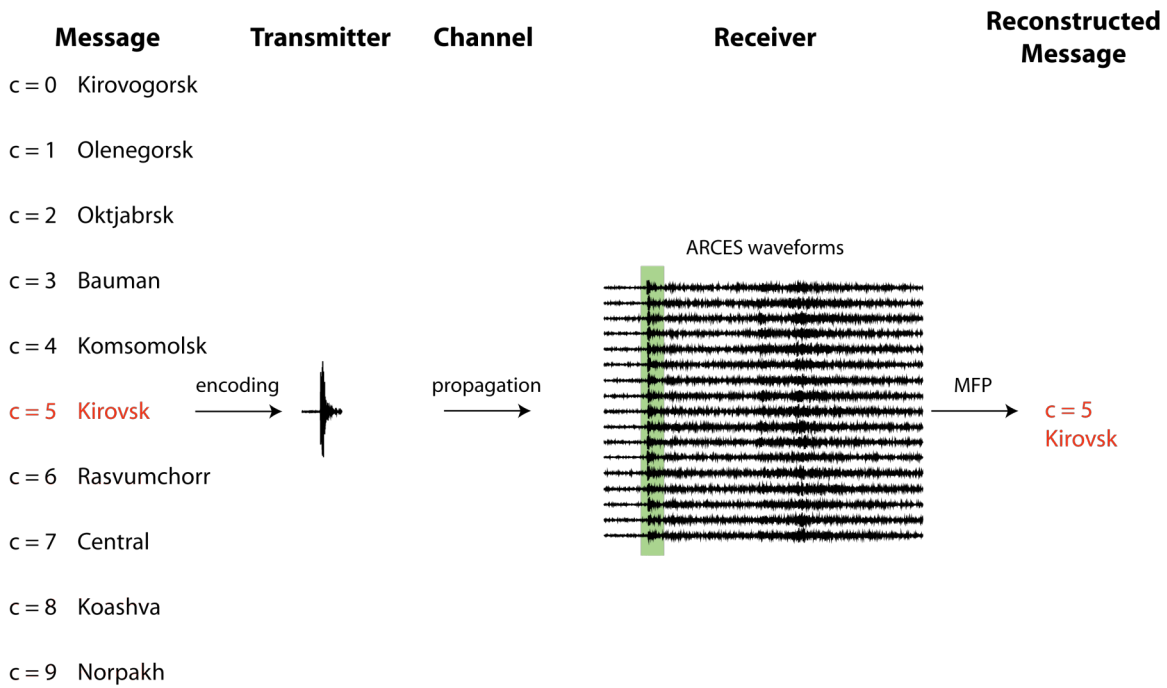


**Figure 2** For purposes of estimating Pn information carrying capacity, the 10 mines of the Khibiny and Olenegorsk groups are considered to be a transmitter conveying information about which source is conducting an explosion. Ten messages are possible. Assuming each mine is equally likely to be the source of any given shot, the messages can be represented with between 3 and 4 (actually  $\log_2(10) = 3.32$  on average) bits of information. The information is encoded in an outgoing seismic wavefield, which propagates over a noisy channel (the earth) to the receiver (the ARCES array) and is there decoded by matched field processing (MFP) to reconstruct the original message. The mutual information between the received ARCES waveforms and an index variable ( $c$ ) indicating the source defines the information conveyed over the channel.

## Frequency domain signal representation

Denote the signals observed at an array element as samples  $x_j[n] = x(r_j, n\Delta t)$  of a continuous signal  $x(r_j, t)$  observed at position  $r_j$ . Let the vector sequence:

$$\underline{x}[n] = \begin{bmatrix} x_1[n] \\ x_2[n] \\ \vdots \\ x_N[n] \end{bmatrix} \quad (1)$$

collect the signals from all ( $N$ ) array elements.

Figure 3 shows an collection of waveforms from explosions at one mine (Norpakh) recorded at one array sensor (ARA0, the center ARCES element). The figure inset shows detail of the initial portion of the waveforms from six explosions. The Pn waveforms from this source differ significantly from shot to shot, presumably because this is an open-pit mine conducting ripple-fired explosions that differ significantly in details of the number of rows of holes used, row orientation, the firing sequence and so forth. Consequently, the wideband, temporal, fine structure of explosion signals from this mine is not repeatable. However, the spatial structure of the signal observed in narrow bands across the array aperture is repeatable, as was seen in a prior contribution.

A frequency domain representation for the observations suppresses the temporal variations and allows us to extract the spatial structure of the signal. Denote the Fourier series

$$\underline{x}[n] = \sum_k \underline{x}_k e^{\frac{i2\pi kn\Delta t}{T}} \quad (2)$$

Here  $T$  indicates the length of an observation interval encompassing the waveform of interest [Figure 3].

To describe that spatial structure, we treat the array signals as nonstationary sample functions from a random process, one sample per event. The event collection of Figure 3 is a finite sampling of the event ensemble defining the random process. The data are processed in bands that exclude zero frequency, hence:

$$E\{\underline{x}[n]\} = E\{\underline{x}_k\} = \underline{0} \quad (3)$$

The spatial structure of the signals is revealed in the covariance of the Fourier coefficients:

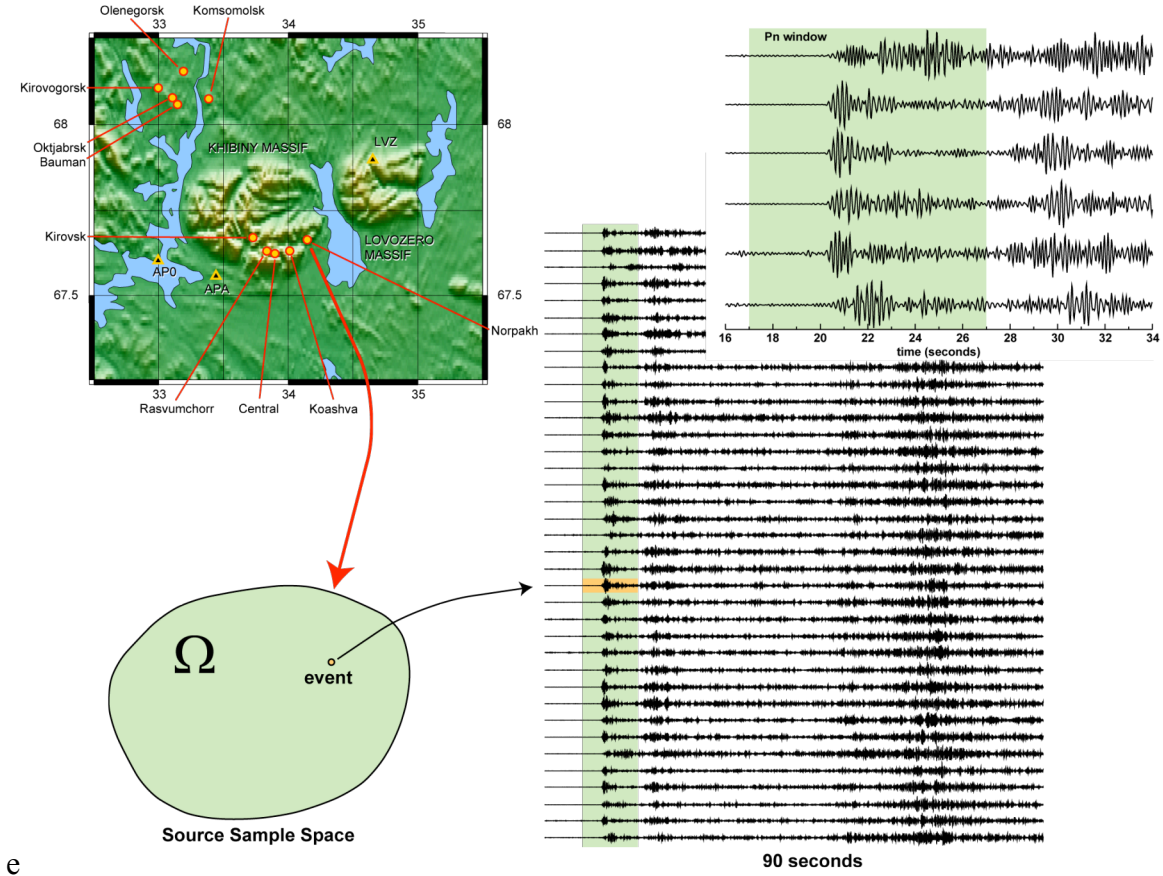


**Figure 3** Seismic signals from events at a repeating source are considered to be sample functions of a transient random process. Each source (the Norpakh mine in this case) has an associated sample space  $\Omega$  from which events are selected at random. The frequency of occurrence or likelihood of points in the sample space is described by a probability density function. Each point in the sample space is associated with a resultant waveform observed by a seismic sensor. The observation space is the collection (ensemble) of all waveforms associated with points in the sample space. In characterizing a source, this ensemble is approximated with a finite sample (a finite number) of observed waveforms. The waveforms shown here have been filtered into the 4 to 8 Hz band for display.

$$E \{ \underline{x}_k \underline{x}_k^H \} = \underline{R}(\omega_k) \quad \omega_k = \frac{2\pi k}{T} \quad (4)$$

The Fourier coefficients can be shown to have the following structure:

$$\underline{x}_k \approx \underline{g}(\omega_k) f(\omega_k) \quad (5)$$

where  $\underline{g}(\omega_k)$  is the vector of Fourier transforms of Green's functions describing propagation from the source, in this case a particular mine, to the elements of the array.

The driving functions  $f(\omega_k)$  denote the source excitation, which is assumed to be a random process and gives the set of observations their random character. The covariance of the Fourier coefficients then is:

$$\underline{R}(\omega_k) = E \left\{ f(\omega_k) f^H(\omega_k) \right\} \underline{g}(\omega_k) \underline{g}^H(\omega_k) = \sigma^2(\omega_k) \underline{g}(\omega_k) \underline{g}^H(\omega_k) \quad (6)$$

Plane wave propagation provides an illustrative example. In this simple case, the Greens' functions are delta functions which introduce signal delays proportional to the propagation time to each element of the array. In the frequency domain:

$$\underline{g}(\omega_k) \propto \begin{bmatrix} e^{-i\omega_k \underline{s} \cdot \underline{r}_1} \\ e^{-i\omega_k \underline{s} \cdot \underline{r}_2} \\ \vdots \\ e^{-i\omega_k \underline{s} \cdot \underline{r}_N} \end{bmatrix} \quad (7)$$

The  $mp^{th}$  element of the covariance matrix in this case is:

$$R_{mp}(\omega_k) \propto e^{-i\omega_k \underline{s} \cdot (\underline{r}_m - \underline{r}_p)} \quad (8)$$

The indicated spatial structure of the signal is shown in Figure 4. In the figure, the amplitudes and phases of the vector of Fourier coefficients are displayed, in the center diagram, with circular symbols at the positions of the array elements. The sizes of the circles represents the amplitudes and the colors the phases. For a plane wave, the amplitudes are uniform across the array, hence the symbols have uniform size. The phase advances in linear bands of constant phase perpendicular to the direction of propagation. The elements of the covariance matrix are rendered in the same fashion on the right side of Figure 4. The covariance of the incident wavefield is sampled on the coarray of the array, which consists of all vector separations pairwise between array elements (equation 8). The structure of the wavefield is more easily discerned on the coarray since there are many more samples of the covariance function on the coarray.

### Observed Spatial Correlation

The mines of the Kola Peninsula provide an opportunity to examine the spatial structure of signal covariance since a large number of ground truth explosions are available to estimate ensemble properties. The procedure for forming estimate is straightforward. For a particular event, indexed by  $l$ , the observed signals are windowed to isolate the Pn phase, then transformed to the frequency domain to obtain sample Fourier coefficients:

$$\underline{x}_k^l = \sum_n \underline{x}^l[n] w[n] e^{\frac{-i2\pi kn \Delta t}{T}} \quad (9)$$

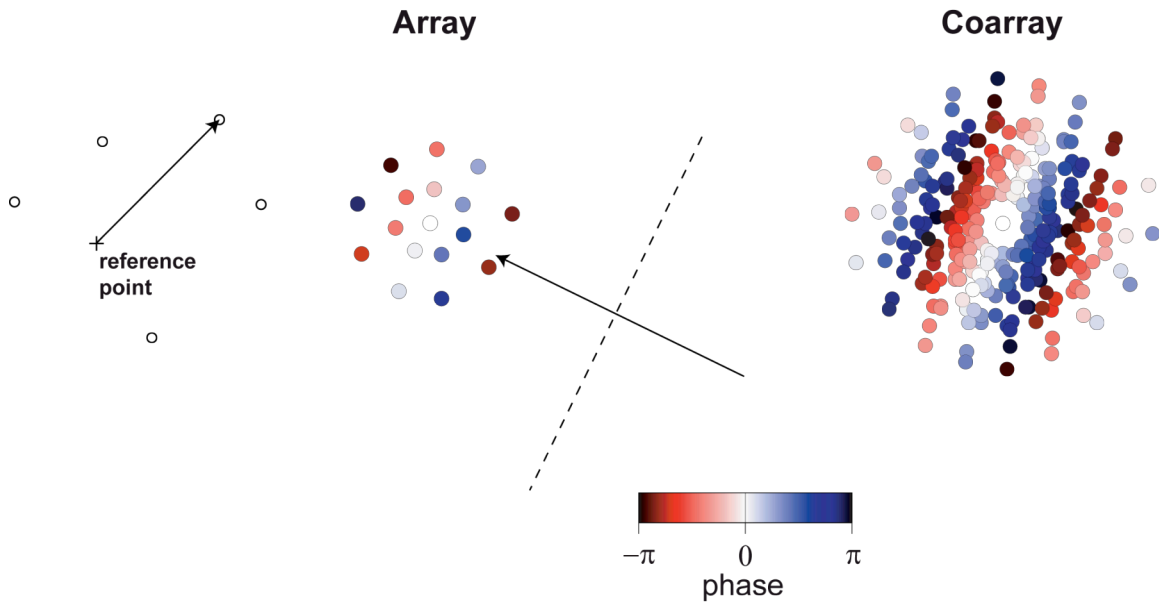


**Figure 4** Graphical representations of a monochromatic plane wavefield incident upon an array enable visualization of spatial structure. In the center, the phase and amplitude structure of a theoretical incident plane wave is depicted with circular symbols at each array element location. The size of the symbol is proportional to the amplitude of the signal and the color encodes the phase. The time history is a complex exponential and is not depicted. At right, the spatial covariance of the signal is depicted in a similar fashion, with the difference that a symbol appears at each coarray location, i.e. at the set of vector differences of array element locations. The planar structure of the signal is apparent from bands of constant phase perpendicular to the direction of propagation. The wavelength of the incident field corresponds to the separation between bands of like color.

The estimate of the ensemble covariance is obtained by averaging the outer product of the sample Fourier vectors:

$$\hat{R}(\omega_k) = \frac{1}{L} \sum_T \mathbf{x}_k^l (\mathbf{x}_k^l)^H \quad (10)$$

and normalizing by the number ( $L$ ) of sample events.

The theoretical covariance matrices for Pn waves observed by ARCES for the 5 mines of the Khibiny Massif are shown in Figure 5, and contrasted with the measured covariance for the same 5 mines in Figure 6. For purposes of this note, the most important feature of Figure 5 is the great uniformity of the spatial covariance among the 5 mines. This observation is true even at the highest frequency (12.5 Hz) depicted. By contrast, the measured covariance ( $L \sim 100$ ) for these mines is relatively uniform below 7 Hz, but becomes strongly diverse at higher frequencies. This diversity is a consequence of scattering under real as opposed to idealized propagation conditions.

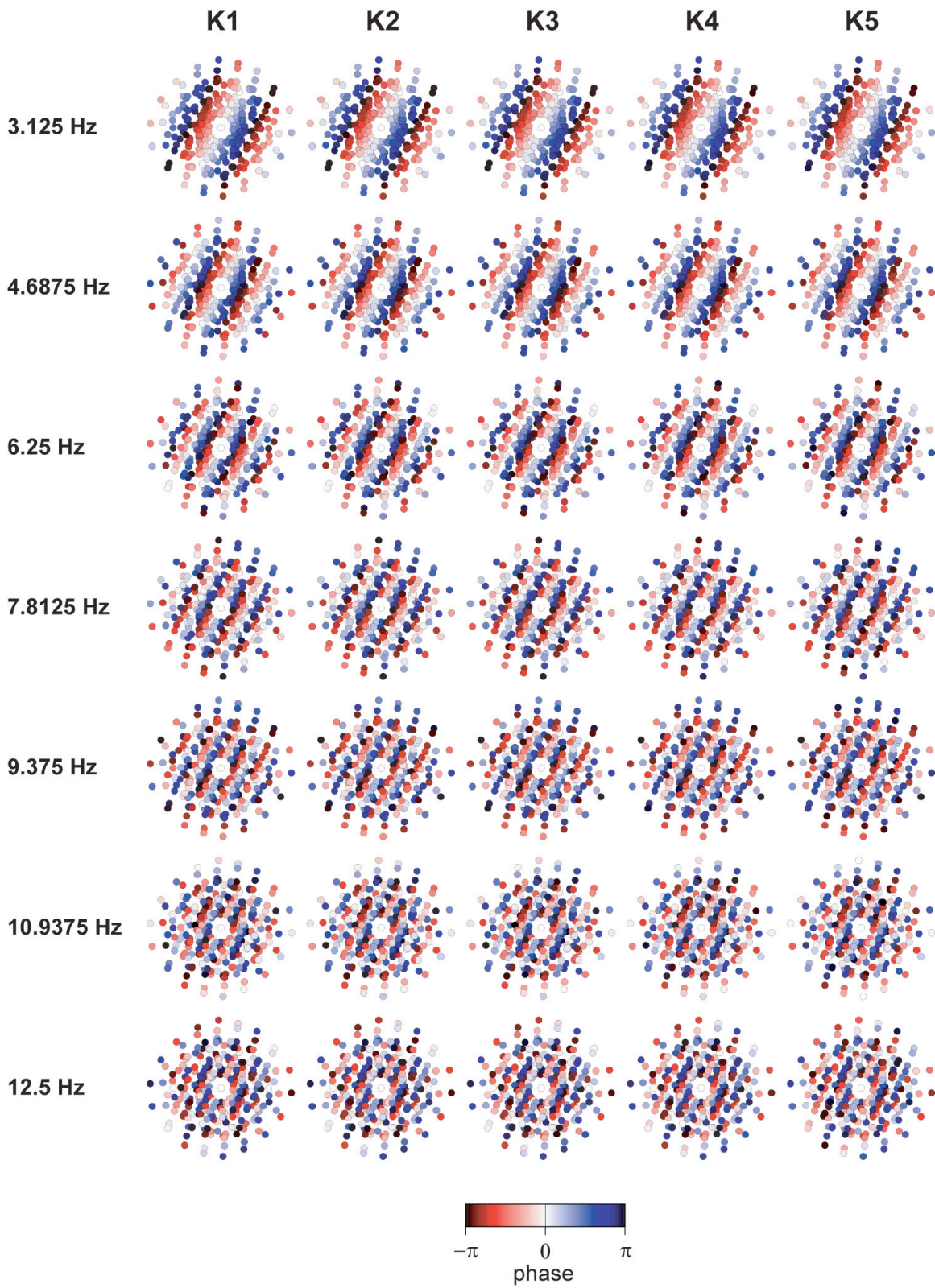


**Figure 5** The pattern of theoretical spatial correlations under a plane-wave model for the five Khibiny mines. Note the great similarity of correlations among the mines.

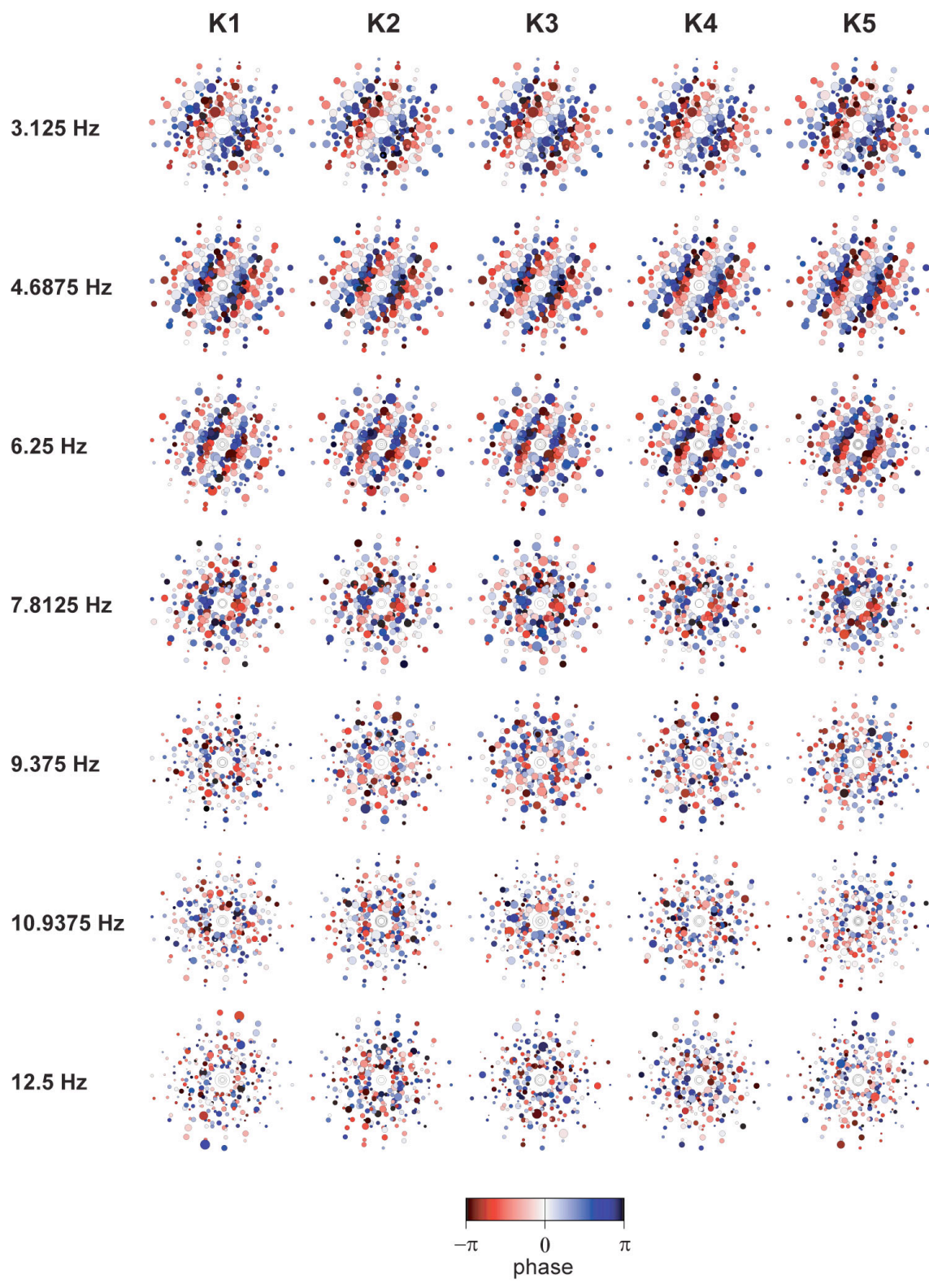


**Figure 6** The pattern of measured correlations for the Khibiny mines corresponding to the theoretical patterns of Figure 5. Note increased spatial diversity at high frequencies.

A number of other real-world propagation characteristics are evident in Figure 6. The correlations become smaller at high frequencies and at larger offsets (toward the edges of the diagrams), which is a general indication of decreasing coherence. The structure of the phase becomes apparently disordered, at least when contrasted with the theoretical phase in which planar structure is detectable to a degree at higher frequencies. The diversity of structure in the observed wavefields increases the information content of the Pn phase and provides an opportunity to distinguish the events at the mines.

### Signal probability model and mutual information

Estimates of the information carrying capacity of the Pn phase require a joint probability density for the observations and some variable indicating the state of the source. We choose a discrete index variable  $c \in [0, 1, \dots, 9]$  to indicate which mine has conducted a particular explosion. We also assume a uniform probability mass function  $p_c = 1/10 \quad \forall c$  for the index variable which indicates that explosions are equally likely to occur at any of the mines. Finally, to develop closed-form results, we assume that the joint density of  $c$  and the observations is complex multivariate normal:

$$p(\underline{x}, c) = p(\underline{x}|c)p_c = p_c \prod_{k=1}^{N_f} |\pi R_c(\omega_k)|^{-1} e^{-\underline{x}_k^H R_c^{-1}(\omega_k) \underline{x}_k} \quad (11)$$

Here the symbol  $\underline{x}$  collects all components  $\{\underline{x}_k; k \in [1, 2, \dots, N_f]\}$  of the Fourier representation of the data. Note that the covariance matrix now is indexed by  $c$  to indicate the signal structure appropriate to a particular mine.

The source, considered as a transmitter of information, assumes one of ten equally likely states. The state can be described by its entropy [Shannon, 1948]

$$-\sum_c p_c \log_2(p_c) \approx 3.32 \quad (12)$$

which is equal to the number of bits of information required, on average, to encode the state of the source. The information conveyed by the observations  $\underline{x}$  about the value of  $c$  is given by the *mutual information* [Shannon, 1948], defined for our problem by:

$$I(\underline{x}, c) = \sum_c \int d\underline{x} p(\underline{x}, c) \log \left\{ \frac{p(\underline{x}, c)}{p(\underline{x})p_c} \right\} = \sum_c \int d\underline{x} p(\underline{x}, c) \log \left\{ \frac{p(\underline{x}|c)}{p(\underline{x})} \right\} \quad (13)$$

The mutual information ranges between zero (when the observations and the index variable are unrelated, i.e.  $p(\underline{x}, c) = p(\underline{x})p_c$ ) and the entropy (information) of the source itself.

Unfortunately, the mutual information cannot be evaluated in closed form for any but the simplest problems. An alternative is to seek bounds on the mutual information that are

sufficiently tight to allow useful inferences about information carrying capacity of our particular channel.

Such bounds on the mutual information have been reported by Haussler and Opper []:

$$-\sum_{c^*} p_{c^*} \ln \left\{ \sum_c p_c \left( 1 - \frac{1}{4} \Delta_H(c, c^*) \right)^n \right\} \leq I(x, c) \quad (14)$$

and:

$$I(x, c) \leq -\sum_{c^*} p_{c^*} \ln \left\{ \sum_c p_c e^{-n \Delta_K(c, c^*)} \right\} \quad (15)$$

Where the (squared) Hellinger distance is defined by:

$$\Delta_H(c, c^*) = 4 \left( 1 - \int dx \left[ p(x|c) p(x|c^*) \right] \right)^{1/2} \quad (16)$$

And the Kullback-Leibler (KL) divergence is defined by:

$$\Delta_K(c, c^*) = \int dx p(x|c) \ln \left\{ \frac{p(x|c)}{p(x|c^*)} \right\} \quad (17)$$

It is beyond the scope of this note to evaluate these bounds for our particular data probability model. We simply state the result. For the covariance model, the Hellinger distance is:

$$\Delta_H(c, c^*) = 4 \left( 1 - \prod_{i=1}^{N_f} \left| \frac{1}{2} \left( R_{c^*}^{1/2}(\omega_i) R_c^{-1/2}(\omega_i) + R_{c^*}^{-1/2}(\omega_i) R_c^{1/2}(\omega_i) \right) \right| \right)^{-1} \quad (18)$$

and the KL divergence is:

$$\Delta_K(c, c^*) = \sum_{i=1}^{N_f} \left[ \ln \left( \frac{|R_{c^*}(\omega_i)|}{|R_c(\omega_i)|} \right) + \text{tr} \left\{ R_{c^*}^{-1}(\omega_i) R_c(\omega_i) \right\} - N_s \right] \quad (19)$$

The detailed derivations will be provided in a future contribution, including forms for the theoretical plane wave case, which provide useful insights into the meaning of the bounds. However, we have evaluated these bounds for the theoretical plane wave covariance structures of Figure 5 and the measured covariances of Figure 6. These results are summarized in Figure 7. In computing the bounds, we have modified the covariance matrices by adding a diagonal matrix representing uncorrelated white noise of varying power. The bounds on mutual information are represented as a function of signal to noise ratio.

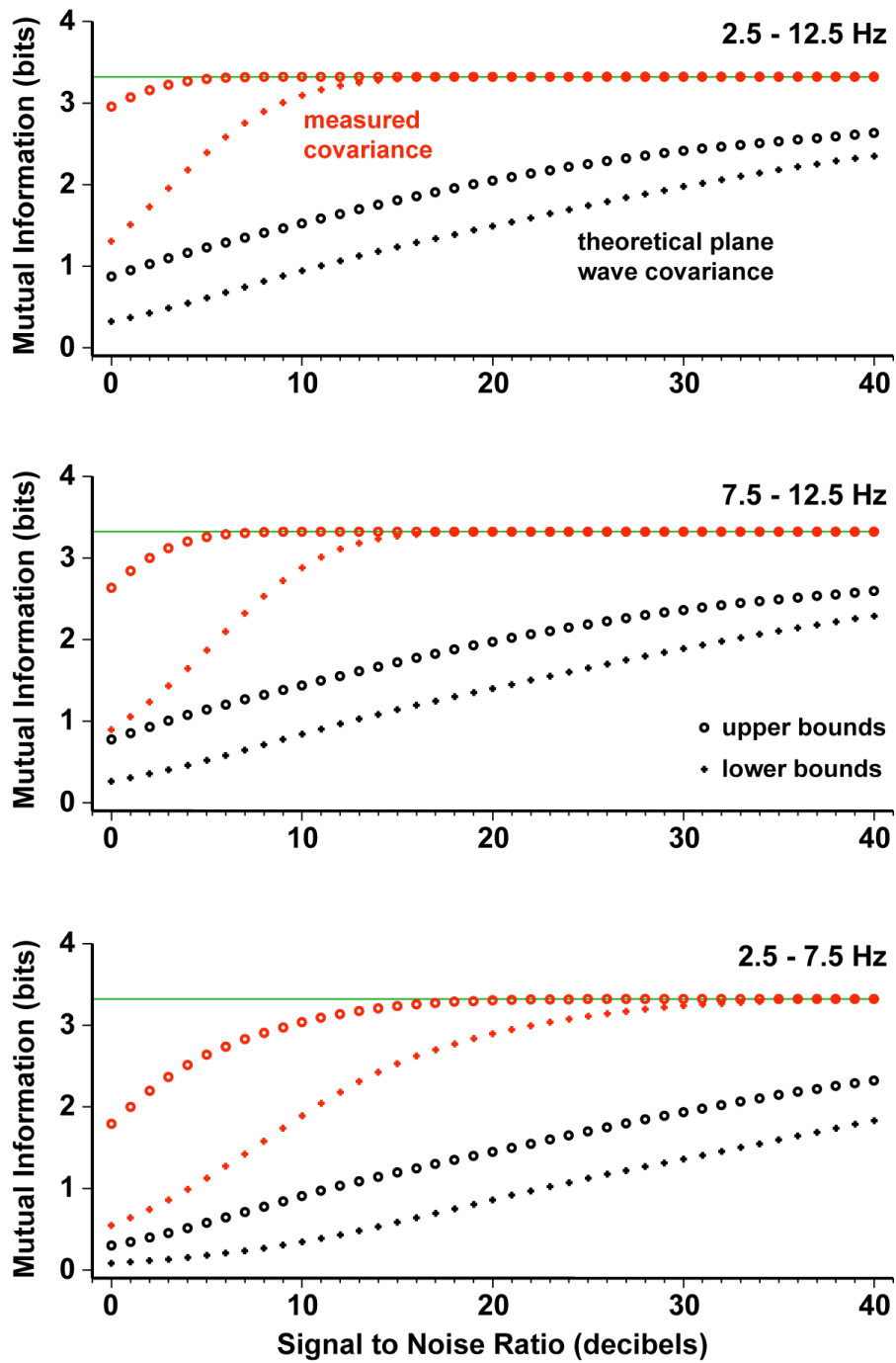


**Figure 7** Bounds on the mutual information for both measured signal covariance structures (red) and theoretical plane-wave covariance structures (black) for the problem of identifying explosions from the ten mines of the Kola peninsula. Three frequency bands are considered: a low band (2.5-7.5 Hz, bottom), a high band (7.5-12.5 Hz, middle) and a wide band (2.5-12.5 Hz, top). The measured covariance, incorporating effects of realistic wave propagation has higher information content.

Three cases are shown in the figure to make a point about the portion of the spectrum where the information is concentrated. The top set of curves shows the upper (circles) and lower (crosses) bounds on mutual information under the measured covariances (red) and the theoretical plane wave covariance (black) for the wideband case (2.5-12.5 Hz). This set provides the principal result that the mutual information under real-world propagation conditions is substantially greater than predicted by free-space (plane wave) propagation conditions. The middle and bottom frames display mutual information bounds for the high band (7.5-12.5 Hz) and the low band (2.5-7.5 Hz) respectively. These bands were chosen to highlight the portions of the spectrum for which the measured covariance was relatively diverse and uniform correspondingly. The point of these plots is that the information gains at low SNR are larger at high frequencies where measured signal diversity is greatest. Consequently, our interpretation is that scattering is responsible for the increase in information content observed under real-world propagation conditions. Certainly scattering is more pronounced at high frequencies.

It is interesting to see that the mutual information predicted for the plane wave model does not achieve the intrinsic information (entropy) of the source even at high SNR (40dB). By contrast, the mutual information under realistic propagation conditions reaches the entropy of the source at 10dB. This is another way to describe the lack of resolution of the array for this particular mine group under perfect propagation conditions, and the superresolution (greater than the Rayleigh limit) afforded by matched field processing. Matched field calibrations capture the increase in information content available in the scattered field, thus enabling superresolution. And they do so, apparently, without sensitivity to the temporal structure of the signal, which defeats classification by waveform correlation methods.

## References

Haussler, D. and M. Opper (1995), General bounds on the mutual information between a parameter and  $n$  conditionally independent observations, Proc. of the Eighth Annual Conference on Computational Learning Theory (ACM), 402-411.

Shannon, C. E. (1948), A mathematical theory of communication, *The Bell System Technical Journal*, **27**, 379-423, 623-656.

## Auspices

This work performed under the auspices of the U.S. Department of Energy by Lawrence Livermore National Laboratory under Contract DE-AC52-07NA27344.